

Anomalous Aharonov-Bohm conductance oscillations from topological insulator surface states

Yi Zhang^{1,2} and Ashvin Vishwanath^{1,2}

¹*Department of Physics, University of California at Berkeley, Berkeley, CA 94720, USA*

²*Materials Sciences Division, Lawrence Berkeley National Laboratory, Berkeley, CA 94720, USA*

(Dated: May 21, 2010)

We study transport properties of a topological insulator nanowire when a magnetic field is applied along its length. We predict that with *strong* surface disorder, a characteristic signature of the band topology is revealed in Aharonov Bohm (AB) oscillations of the conductance. These oscillations have a component with anomalous period $\Phi_0 = hc/e$, and with conductance maxima at odd multiples of $\frac{1}{2}\Phi_0$, i.e. when the AB phase for surface electrons is π . This is intimately connected to the band topology and a surface curvature induced Berry phase, special to topological insulator surfaces. We discuss similarities and differences from recent experiments on Bi_2Se_3 nanoribbons, and optimal conditions for observing this effect.

PACS numbers:

There has been much recent interest in Topological Insulators (TIs), three dimensional solids which are insulating in the bulk but display protected metallic surface states (see [1] for reviews), in the presence of time reversal (\mathcal{T}) invariance. Surface sensitive experiments such as ARPES and STM [1], have confirmed the existence of this exotic surface metal. However, so far there have been no transport experiments verifying the topological nature of the surface states. Besides the fact that bulk impurity bands may contribute significantly to conductivity, the key transport property is the absence of localization when \mathcal{T} invariance is present. This has been hard to convert into a clear-cut experimental test. Here we discuss a topological feature of TI surface states that can lead to a transport signature.

Consider a wire of topological insulator, with magnetic flux applied along its length. The surface states can be considered a collection of one dimensional modes, that come in pairs moving up and down the wire. Time reversal symmetry is present at zero flux, and also, approximately for the surface states, when the surface encloses an integer multiple of $\frac{1}{2}\Phi_0$ ($= hc/2e$) flux quanta. However, there is an important difference between even and odd multiples of $\frac{1}{2}\Phi_0$ -flux. Odd multiples of $\frac{1}{2}\Phi_0$ -flux leads to a π Aharonov-Bohm phase for surface electrons, resulting in an odd number of pairs of modes. This one dimensional state is topologically protected and cannot be localized with \mathcal{T} symmetry[2]. In contrast, even multiples of $\frac{1}{2}\Phi_0$ -flux leads to an even number of modes which are not protected. Thus, with sufficiently strong disorder, even flux leads to a fully localized state for a long wire while odd flux leads to a metallic state whose conductance approaches $2e^2/h$, under ideal conditions. Interestingly, as discussed below, a crucial component of this even-odd effect is a surface curvature induced π Berry's phase. Throughout we assume low temperatures so the thermal dephasing length exceeds the sample dimensions.

Note, this oscillatory dependence has a flux hc/e pe-

riod, in contrast to Aharonov-Altshuler-Spivak (AAS) oscillations which have period $hc/2e$. There has been much discussion on the question of hc/e vs $hc/2e$ oscillations, in mesoscopic rings[3, 4] and cylinders [5, 6]. For rings, both periods are observed, the first period is attributed to AB interference of single electrons, and the second to AAS oscillation arising from weak localization effects. However in metallic cylinders, only the $hc/2e$ period has been experimentally reported [5]. The hc/e period has been theoretically predicted, [4, 6], but always occurs with random sign, i.e. they can peak at either even or odd multiples of $\frac{1}{2}\Phi_0$. Therefore an ensemble average tends to wash out this effect, which, according to Ref. [3, 4], is why the $hc/2e$ effect is more commonly observed.

In contrast, the hc/e oscillation described here are unique in having maxima always at odd-integer multiples of $\frac{1}{2}\Phi_0$, and only occur in strong topological insulators.

A recent experiment on topological insulator Bi_2Se_3 nanowires has indeed reported such an anomalous hc/e flux period [7]. However, there is a crucial difference from the effect described above - the conductivity is found to be minimum at the locations of the predicted maxima. Hence Ref. [7] is presumably observing different physics, explaining which is an interesting open question. The regime described in this paper is best accessed by going to strong disorder on the surface, or by enhancing the one dimensional nature of the system, eg. by considering narrower wires. We believe this regime could well be accessed by future experiments of a similar nature.

We first describe the physical ingredients that give rise to this anomalous AB effect, such as curvature induced Berry phase, in clean systems. Subsequently we report the result of numerical experiments on disordered cylinders of topological insulators, realized in a three dimensional lattice model. Strong disorder is confirmed to expose this anomalous AB effect.

A single Dirac cone is the simplest model of TI surface states, which naturally invites comparison with

graphene, with a pair of Dirac nodes centered at momenta $\pm K$, for each spin projection. If scattering between the graphene's nodes are neglected, one might conclude that the topological insulator surface is simply '1/4th' of graphene. Here we point out a topological effect that is special to TI surfaces, connected to the fact that the surface Dirac fermions are sensitive to spatial topology, in the same way as Dirac particles in a curved two dimensional space. There is no analog of this for graphene, even when it is rolled up into curved structures such as nanotubes and buckyballs. The root of this difference can be traced back to the physical interpretation of the Dirac matrices. While in graphene, Dirac matrices act on an internal pseudospin space, in topological insulators they act on physical spin, which are locked to the surface orientation. Hence surface curvature introduces new effects in TIs as described in Ref [8]. In particular, consider an electron circling the cylindrical surface of a topological insulator. Due to the locking of spin to the surface orientation, an additional Berry's phase of π is acquired during such a revolution. The surface modes of a cylinder appear in pairs moving up and down the axis. A consequence of the Berry phase is that there are an *even* number of these pairs. If modes are labeled by angular momenta, k_θ , these are quantized to half integers because of the Berry phase. Thus there is no unpaired low energy Dirac mode at $k_\theta = 0$. In contrast, in carbon nanotubes, the $k_\theta = 0$ mode is present and responsible for the metallicity of eg. armchair nanotubes. Now, if an additional Aharonov-Bohm flux of π threads the cylinder of topological insulator, canceling the curvature Berry's phase, one reverts to the regular quantization i.e. $k_\theta = 0$ is allowed, and hence an odd number of one dimensional mode pairs are present (see Fig. 1a,b).

Surface Dirac Theory: Consider generalizing the Dirac Hamiltonian for a flat surface perpendicular to the z direction, $H = -iv_F\hbar(p_x\sigma_x + p_y\sigma_y)$ to the case when the surface is curved. We utilize the fact that the surface is embedded in three dimensional space, so $\mathbf{r}(x^1, x^2)$ is the three vector defining the surface location, as the coordinates x^i ($i = 1, 2$) are varied. Then, $\mathbf{e}_i = \partial\mathbf{r}/\partial x^i$ are tangent vectors. Define conjugate tangent vectors \mathbf{e}^i , via $\mathbf{e}^i \cdot \mathbf{e}_j = \delta_{ij}$, the Kronecker Delta function. Naively, one might guess that the Dirac equation on this curved surface is just: $H_1 = -iv_F\hbar(\alpha^1\partial_1 + \alpha^2\partial_2)$, where $\partial_i = \partial_{x^i}$ and $\alpha^i = \mathbf{e}^i \cdot \boldsymbol{\sigma}$ are the Pauli matrices along the tangent vectors. However, the actual form is a little more involved, and is most compactly written if we assume x^i are *normal* (also called geodesic) coordinates. In these coordinates, (i) the \mathbf{e}^i are orthonormal $\mathbf{e}^i \cdot \mathbf{e}^j = \delta_{ij}$; and (ii) the derivatives: $\partial\mathbf{e}^i/\partial x^j$, are along the surface normal $\mathbf{e}^3 (= \mathbf{e}^1 \times \mathbf{e}^2 / |\mathbf{e}^1 \times \mathbf{e}^2|)$. The coefficients of proportionality are the principal curvatures $\partial\mathbf{e}^i/\partial x^j = -\frac{\delta_{ij}}{R_i}\mathbf{e}^3$. Such a set of coordinates can always be found locally. In these coordinates it is readily established that there is an

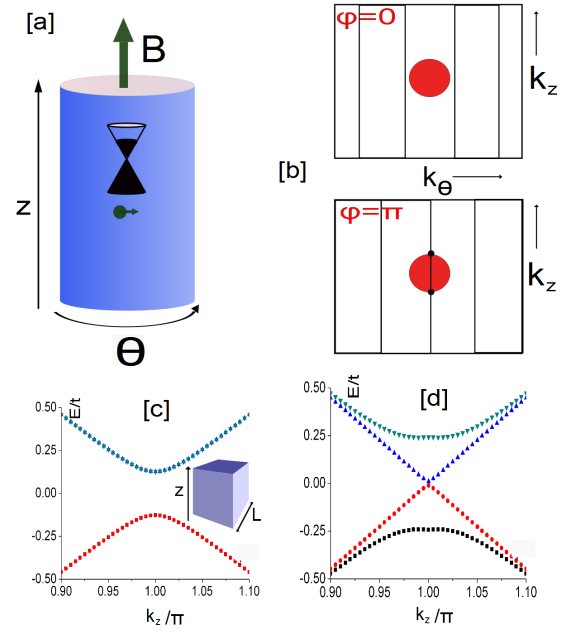


FIG. 1: (a) proposed geometry, with (weak) magnetic field applied along the wire axis, with flux $\varphi = 2\pi\Phi/\Phi_0$ enclosed. (b) Quantization of transverse momenta k_θ for a cylinder, as a function of applied flux. The shaded area boundary in the Fermi surface. For $\varphi = 0$, an even number of 1D mode pairs occurs; but with $\varphi = \pi$ flux, an odd number of pairs, protected by time reversal symmetry, is expected. Demonstration in a microscopic model: spectrum of a cuboid of clean topological insulator, with cross section 10x10 unit cells (geometry shown in inset), as a function of momentum k_z along its length. (c) Spectrum for $\varphi = 0$, each band shown is doubly degenerate (d) For flux $\varphi = \pi$, all modes except the linear one are doubly degenerate; hence an odd number of 1D mode pairs is present.

additional term:

$$H_D = -iv_F\hbar(\alpha^1\partial_1 + \alpha^2\partial_2) + i\frac{\hbar v_F}{2}\left(\frac{1}{R_1} + \frac{1}{R_2}\right)\beta \quad (1)$$

where $\beta = \mathbf{e}^3 \cdot \boldsymbol{\sigma}$. A shortcut to obtaining it is requiring that the Hamiltonian H_D be Hermitian and also anticommute with the local β matrix (note, the matrices α^i , β are space dependent).

A more formal derivation of the same result proceeds from the general form for a Dirac equation in curved space: $H_D = -i\hbar v_F(\alpha^1 D_1 + \alpha^2 D_2)$, where D_i is the covariant derivative along a pair of general coordinates x^i , defined as $D_i = \partial_i + \Gamma_i$, where Γ_i is the spin connection, which here is given by the equation:

$$[\Gamma_i, \alpha^j] = \partial_i \alpha^j + \Gamma_{ik}^j \alpha^k \quad (2)$$

where $\alpha^k = \mathbf{e}^k \cdot \boldsymbol{\sigma}$, and summation over repeated indices is assumed. The Γ_{ik}^j are the Christoffel symbols. This can be solved explicitly to give the following simple ex-

pression:

$$\Gamma_i = -\frac{1}{2}\beta\partial_i\beta \quad (3)$$

The Christoffel symbols are defined from the derivatives of the tangent vectors, projected into the tangent plane: $[\partial_i \mathbf{e}^j]_{\parallel} = -\Gamma_{ik}^j \mathbf{e}^k$ (indices take on values $\in \{1, 2\}$) [9]. Now, we switch to normal coordinates. Clearly, the Christoffel symbols vanish since the derivatives of the tangent vector are now normal to the surface. Thus from Eqn. 2 the spin connection is given by $\Gamma_{1,2} = \pm \frac{i}{2R_{1,2}} \alpha^{2,1}$, which leads back to Eqn. 1. An alternate elegant formalism is developed in Ref. [10], for quantized Hall states.

Now, let us specialize to a cylindrical surface such that $x^1 = z$ along the cylinder axis and $x^2 = R\theta$, where R is the radius and θ is the angle around the cylinder. Now, $R_1 = \infty$ and $R_2 = R$, in Eqn. 1. The unitary transformation $U = e^{i\sigma_z\theta/2}$, transforms that into the canonical form $H'_D = -i\hbar v_F(\sigma_z\partial_z + \sigma_y\partial_\theta/R)$. However, since the unitary transformation changes sign $\theta \rightarrow \theta + 2\pi$, the wavefunctions for the new Hamiltonian satisfy *antiperiodic* boundary conditions on circling the cylinder. Therefore, only angular momenta $\hbar(m+1/2)$ are allowed, where m is integer. Hence, the zero angular momentum is absent, and there are an even number of one dimensional modes pairs. Now threading an additional π flux, the periodic boundary conditions are restored, and the parity of the mode pairs is reversed; see [9] for a more general argument. Although the cylinder has vanishing Gaussian curvature, a nonzero spin connection leads to the Berry's phase of π . This topological property is also ultimately responsible for metallic dislocation lines [8, 11].

Microscopic Model: We now demonstrate this effect for a lattice model of a strong topological insulator (which is more general than the Dirac approximation). We use the model of Fu-Kane-Mele [12] on the diamond lattice

$$H = \sum_{\langle aij \rangle} t_{ij} c_{i\sigma}^\dagger c_{j\sigma} + 8i\lambda_{SO} \sum_{\langle\langle ik \rangle\rangle} c_{i\sigma}^\dagger (\hat{\mathbf{d}}_{ik}^1 \times \hat{\mathbf{d}}_{ik}^2) \cdot \mathbf{s}_{\sigma\sigma'} c_{k\sigma'} \quad (4)$$

Parameters are chosen to give a strong topological insulator [9] with bulk gap $\Delta = 2t$. A long cuboid with cross section $L \times L$ is taken along the weak index direction of this model, and surface states are labeled by momenta k_z along the long axis. A uniform magnetic flux Φ is introduced uniformly through the cross section, denoted in units of the flux quantum: $\varphi = 2\pi\Phi/\Phi_0$. The surface spectrum is shown in Fig. 1. All modes are doubly degenerate except the linearly dispersing mode in 1 d. Thus, even for small sizes $L = 10$, the even-odd mode effect and the gap closing at flux $\varphi = \pi$ is apparent. While the breaking of time reversal symmetry at this flux implies there is always a gap, this is seen to be very small, and the curves appear 2π periodic, so time reversal is approximately a good symmetry at these flux values. Thus,

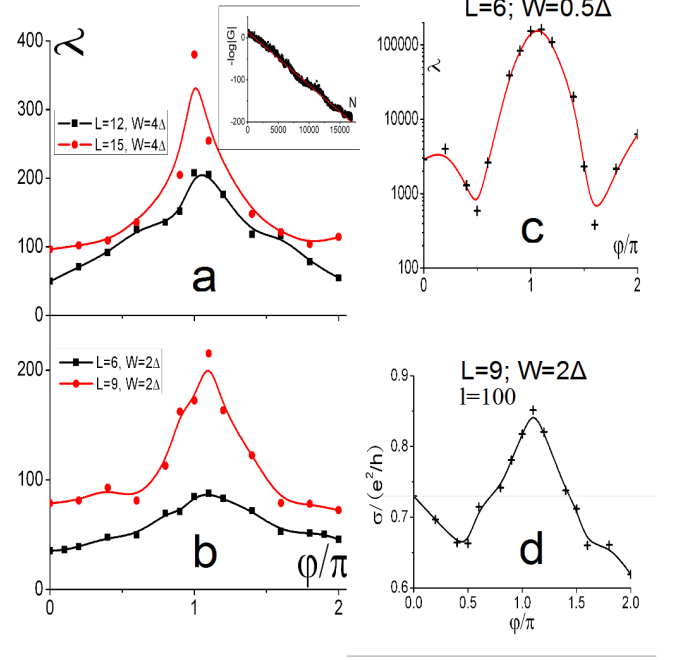


FIG. 2: (a), (b) and (c): Localization length λ in the quasi one dimensional geometry, for different widths L (measured in unit cells) and disorder strengths W (in units of the bulk gap Δ). Error bars are smaller than the symbol size. (a) and (b) Strong disorder: variation has flux-period hc/e and λ is maximum at flux $\varphi = \pi$. Inset: Example of the exponential decay of the Green's function used to determine the localization length. (c) Weak disorder: Now, the $hc/2e$ oscillation period is also apparent and localization lengths are very large (note log scale here). For wires much shorter than the zero flux localization length, the hc/e period will not be apparent. (d) Conductance Oscillation: Direct measure of conductance oscillation for a wire of length $l = 100$ and width $L = 9$, with strong disorder $W = 2\Delta$. Maximum conductance occurs at π -flux.

even in the clean limit, metallic behavior appears at odd multiples of π flux, for a carefully tuned chemical potential near the node. However, on raising the Fermi energy, the flux strength with the larger number of modes oscillates between flux zero and π . A robust response however is exposed by the presence of strong disorder, which we discuss next.

Disordered System: We now consider adding disorder *only* on the surfaces of the model above, via a random onsite potential $V_i n_i$, (\mathcal{T} invariant disorder), where n_i is the charge density onsite, and V_i a random variable picked from a box distribution $[-W, W]$. We calculate the Greens function for a system composed of N layers in the z direction, and transverse size $L \times L$, at energy E : $G_N(r, r'; E)$. The position and spin coordinates are lumped into r . The transport properties of the surface states are characterized by extracting the localization length of the system in the quasi-one dimensional limit. Subsequently, we will directly calculate the conductiv-

ity. The technical simplification for localization length λ is that one only needs the Greens function between the first and last layers of the system, as the system length is increased. Denote by the matrix $\mathbf{G}_{1,N+1}^{(N+1)}$, the Greens function between the first and last layers of a system with $N+1$ layers, where the matrix indices refer to sites in the layer, and the energy label is suppressed. The localization length: $\lambda^{-1} = \lim_{N \rightarrow \infty} \frac{-2}{N} \log(|\mathbf{G}_{1,N+1}^{(N+1)}|^2)$, which is self averaging, is extracted by a linear fit (an example is shown in figure 2a inset) to the logarithm of the Greens function. The latter can be efficiently calculated [9, 13].

Results are shown in figure 2, where parameters were chosen to obtain a bulk gap $\Delta = 2t$, the hopping strength. System sizes with perimeter $4L$, with $L = 6, 9, 12, 15$ were studied and the quasi 1D localization length $\lambda(\varphi)$ was extracted as a function of flux. We consider strong disorder, to obtain a localization length short enough to be measured: $W = 2\Delta$ for the first two and $W = 4\Delta$ for the last two sizes. The chemical potential was taken to be near the middle of the gap ($E = 0$), where the Dirac node appears in the clean limit. For these strong disorder strengths, results are nearly *independent* of chemical potential location inside the bulk gap. As seen in Figure 2a,b a clear maximum in localization length is seen near $\varphi = \pi$. Note, time reversal is already an approximate symmetry even for the smallest sizes, given the location of the maximum near $\varphi = \pi$ and the $\varphi \rightarrow 2\pi - \varphi$ approximate symmetry. However at $\varphi = \pi$, localization length is finite, so time reversal symmetry breaking enters here. Clearly, for larger widths the symmetry is more accurate, given the weaker fields prevailing on the surface states. If we denote:

$$g_\varphi = \lambda(\varphi)/4L$$

this ranges from $g_0 = 1.6$ to $g_\pi = 6.3$, as the flux is varied, for $L = 15$. Hence, for these parameters, wires with aspect ratios roughly within this range should exhibit conductance oscillations as a function of flux with a maximum at flux π . This is explicitly checked below. We have also checked that the *Zeeman* splitting induced by the field for these sizes do not affect results qualitatively, if their energy scale $E_z \leq 0.025\Delta$, which should be readily satisfied in experiments.

Weak Disorder: In Figure 2d, we plot a system with weak disorder, where $W = 0.5\Delta$, and the chemical potential is tuned to $E = 0.15\Delta$, where there is a large density of states. The localization lengths are now significantly longer (note the log scale for λ), and a prominent anti-localization feature is present near flux $\varphi = \pi/2, 3\pi/2$. The latter will contribute to an AAS $hc/2e$ period in conductance oscillations. Since $g_0 = 125$, at smaller aspect ratios the system is unaware that there is an even longer localization length at π flux, and the most visible feature is likely to be the $hc/2e$ AAS oscillations. This illustrates the important role of strong disorder in observing

the effect of interest.

Conductance: Finally, in Figure 2d, we present the conductance of a wire with length $l = 100$, cross section 9×9 and strong disorder strength $W = 2\Delta$. The conductance is extracted from the Greens function using the Kubo formula, $\sigma = \frac{e^2 \hbar}{\pi l^2} \text{Tr} [v_z \text{Im} \mathbf{G} v_z \text{Im} \mathbf{G}]$ with $v_z = \frac{i}{\hbar} [H, z]$. The effect of leads is modeled by sandwiching the disordered system between 4×10^3 layers of clean wire on either side. We take $\mu = 0.15\Delta$, to obtain a finite density of states in the leads. The localization length for these parameters is close to that in Figure 2b, so l is intermediate between the localization lengths obtained there. A small imaginary part $\epsilon \sim 5 \times 10^{-4}\Delta$ is inserted in the energy to obtain finite results; results are insensitive to its precise value. Each data point is obtained by averaging log of conductance over 500 samples. Clearly, a conductance maximum at flux π is observed. Note however, the $hc/2e$ oscillations are more prominent here than in the localization length plots, and the overall contrast in conductance is of order $0.1e^2/h$. This will increase for longer wires and wider cross sections, where the effects of \mathcal{T} breaking at π flux are less important, and localization of states away from this flux will set in. While a more extensive conductance analysis is left to the future, these results corroborate the basic picture.

Scaling Analysis: How do these results scale to experimentally relevant system sizes, and in particular will the effects described here survive? As a reference, we note that a Bi_2Se_3 nanowires studied in Ref. [7], was 350nm in circumference, and about $2\mu\text{m}$ in length. While a direct conversion into unit cell lengths is difficult due to the extreme anisotropy of the material, we estimate aspect ratios (length to circumference) between 5-10. The circumferences themselves are about 5-10 times larger in unit cell lengths, than those considered here. While in the truly two dimensional limit a metallic (symplectic metal) phase is expected, hence $g(L \rightarrow \infty) \rightarrow \infty$, this growth is slow. The scaling to larger widths is captured by the beta function $\beta(g) = d \log g / d \log L$, similar to the well known beta function for conductance. This function is known for spin-orbit metals in 2D [14]. For large g , the topological insulator surface displays identical behavior[15, 16]; i.e. $\beta(g) \sim 0.64/g$. We estimate this to be reasonably accurate for $g \geq 2$ for TI surfaces, then $g(\tau L) \approx g(L) + 0.64 \log \tau$. The localization length ratio for $\tau = 10$ times wider system compared to the $L = 15$ case, will be $g(L = 150) \approx 3.2$ at zero flux, an aspect ratio that is easily exceeded. Note, the localization length at π flux diverges more rapidly, since the effects of \mathcal{T} breaking are weaker at larger widths. It is readily seen that this scales asymptotically as $\lambda(\varphi = \pi) \sim L^4$ (since the time reversal symmetry breaking strength scales as $\delta \sim 1/L^2$, and the localization length for weak \mathcal{T} breaking disorder scales as $\lambda \sim 1/\delta^2$). Thus the oscillatory effects should remain visible at these longer scales, with strong disorder.

Experimental Realization: In [7], nanowires of Bi_2Se_3 were subjected to a field along their length and an oscillatory dependence of conductance $O(e^2/h)$ with applied flux was reported. The oscillation period was consistent with surface states sensing a hc/e flux. However, the conductivity maxima were generally located at integer multiples of the flux quantum, rather than half integer multiples as predicted here. Therefore we believe a different effect is at play there. The main ingredients required to access the π flux effect discussed here is quasi one-dimensionality and strong disorder. The former can be achieved by studying narrower wires; eg. wires with half the width of those studied were produced in [7]. For the latter, one is aiming to reduce the metallicity of the surface layer, which in a Drude model is just $(e^2/h)k_F l$. This can be achieved either by decreasing the scattering length l , via greater surface disorder, or tuning the chemical potential to an energy with smaller carrier density.

Conclusions: We described a topological property of the surface states of TIs. An Aharonov-Bohm phase of π strengthens the metallic nature of surface states, leading to a clear-cut transport signature. Conductance oscillations with flux are expected in nanowires of topological insulator, with maxima at odd-integer multiple of $\frac{1}{2}\Phi_0$. The key requirements for observing this effect are quasi one-dimensionality and strong disorder, which we believe are achievable given current experimental capabilities.

We thank H. Mathur, D. Carpentier, J. Moore, and G. Paulin for insightful discussions. This work was supported by DOE grant DE-AC02-05CH11231. In independent work [18], similar results are obtained using an ideal Dirac dispersion with twisted boundary conditions as a simple model of TI surface states experiencing magnetic flux.

Supplementary Material

1. *Curved Surface Dirac Theory:* Here we remind the reader of general formalism of defining curved spacetime Dirac theories, and then specializing to our case of interest where only the space is curved. We follow reference [17].

Consider flat 2+1 dimensional spacetime. We work with Euclidean time, so $x^0 = \tau = it$, and $\hbar = c = 1$. Then, the massless Dirac equation reads: $(\sum_{a=0}^2 \gamma_a \partial_a) \Psi = 0$. The matrices satisfy the anticommutation relations: $\{\gamma_a, \gamma_b\} = 2\delta_{ab}$, where the right hand side is the Kronecker delta function, due to the Euclidean spacetime. The γ matrices can just be taken as the Pauli matrices, and we can write this as a three vector $\gamma = (\gamma_0, \gamma_1, \gamma_2)$.

Now consider a curved spacetime, defined by coordinates x^μ metric $g_{\mu\nu}$, where the indices take values $\in \{0, 1, 2\}$. It is always possible to define a triad of vectors ϵ_μ , with three components each, such that

$g_{\mu\nu} = \epsilon_\mu \cdot \epsilon_\nu$. One can define also a dual frame ϵ^μ such that $\epsilon^\mu \cdot \epsilon_\nu = \delta_\nu^\mu$, the Kronecker delta function. (This is like the relation between bases in real space and reciprocal space, for a crystal). Now, the generalization of the Gamma matrices can be defined as: $\gamma^\mu = \epsilon^\mu \cdot \gamma$, or in component form $\gamma^\mu = \sum_{a=0}^2 \epsilon_a^\mu \gamma_a$. The Dirac equation in curved space takes the form:

$$\gamma^\mu (\partial_\mu + \Gamma_\mu) \Psi = 0$$

where $\partial_\mu = \partial/\partial x^\mu$, and summation over repeated indices is assumed from here on. The Γ_μ matrices are the spin-connections, the main objects of interest here. They are given most compactly by the formula

$$\Gamma_\mu = \frac{1}{4} \gamma_\nu \nabla_\mu \gamma^\nu \quad (5)$$

$$\nabla_\mu \gamma^\nu = \partial_\mu \gamma^\nu + \Gamma_{\mu\lambda}^\nu \gamma^\lambda \quad (6)$$

$$\Gamma_{\mu\lambda}^\nu = \frac{1}{2} g^{\nu\alpha} (\partial_\mu g_{\alpha\lambda} + \partial_\lambda g_{\mu\alpha} - \partial_\alpha g_{\mu\lambda}) \quad (7)$$

where the Eqn. 5 relates the spin connection to the covariant derivative ∇_μ . This is defined via the usual Christoffel symbols, $\Gamma_{\mu\lambda}^\nu$ (Eqn. 7), which in turn are defined from the metric via the standard formula (Eqn. 7). The spin connection can be shown to satisfy the equation:

$$[\Gamma_\mu, \gamma^\nu] = \partial_\mu \gamma^\nu + \Gamma_{\mu\lambda}^\nu \gamma^\lambda \quad (8)$$

which indicates that it is responsible for parallel transport of spinors.

We now specialize to the case when only space is curved. Then, we expect the metric tensor can be brought into the form $g_{00} = 1; g_{0i} = 0$, where the Latin indices $i, j, k \dots$ will take on values $\in \{1, 2\}$. This can be arranged if ϵ^0 is unit modulus and orthogonal to the other two tangent vectors. Note also, the only non-vanishing Christoffel symbols are ones with all Latin indices Γ_{jk}^i . Similarly the temporal spin connection vanishes $\Gamma_0 = 0$. To read off the Hamiltonian, we write the Dirac equation as $\partial\Psi/\partial\tau = -H\Psi$, where $H = \gamma_0[\gamma_i(\partial_i + \Gamma_i)]$. We therefore identify $\beta = \gamma_0$, and using $\beta^2 = 1$, $\gamma^i = -i\beta\alpha^i$. Substituting this into Eqn. 5, we obtain:

$$\Gamma_i = -\frac{1}{4} (\beta \partial_i \beta + \alpha_k \partial_i \alpha^k + \Gamma_{ik}^j \alpha_j \alpha^k) \quad (9)$$

Actually, an even simpler form for the spin connection is:

$$\Gamma_i = -\frac{1}{2} \beta \partial_i \beta \quad (10)$$

To derive this we first show (i) the spin connection is in the tangent plane, i.e. it can be expressed in

terms of α_i and then (ii) it is given by the expression above.

To do this, its useful to use the relations8. First consider the zeroth component $\gamma^0 = \beta$;

$$[\Gamma_i, \beta] = \partial_i \beta$$

since all the relevant Christoffel symbols vanish. Now, if we can prove that Γ_i are in the tangent plane, then the commutator can be written as $2\beta\Gamma_i = -\partial_i\beta$ which gives us the desired result Eqn. 10. We now prove the assertion that Γ_i lives in the tangent plane. To do this we write equations for α_i :

$$[\Gamma_i, \alpha^j] = \partial_i \alpha^j + \Gamma_{ik}^j \alpha^k$$

which can be derived from Eqn8, and the definition $\alpha^j = i\beta\gamma^j$. Now, if Γ_i only has components in the tangent plane, the right hand side is proportional to β , i.e. it corresponds to the surface normal. We can check therefore that the right hand side has no components in the plane. Note, it corresponds to the vector $\partial_i \mathbf{e}^j + \Gamma_{ik}^j \mathbf{e}^k$. However, we have mentioned before that $[\partial_i \mathbf{e}^j]_{\parallel} = -\Gamma_{ik}^j \mathbf{e}^k$. Therefore the only remaining component is perpendicular to the plane, as we required.

To see this algebraically, we consider the inner product with a general in plane vector \mathbf{e}_l , which gives:

$$\mathbf{e}_l \cdot \partial_i \mathbf{e}^j + \Gamma_{il}^j \quad (11)$$

where we used $\mathbf{e}^k \cdot \mathbf{e}_l = \delta_l^k$. This can be shown to be zero. The critical input in this derivation is that $\partial_i \mathbf{e}_j = \partial_j \mathbf{e}_i$, which is only true because these are tangent vectors, derived by differentiating the three dimensional coordinates of the surface $\mathbf{e}_i = \partial \mathbf{r} / \partial x^i$.

We note identical results are obtained if we choose the basis vectors as a fixed linear combination of tangent vectors: i.e. if $\mathbf{e}'_1 = \cos \theta \mathbf{e}_1 + \sin \theta \mathbf{e}_2$ and $\mathbf{e}'_2 = -\sin \theta \mathbf{e}_1 + \cos \theta \mathbf{e}_2$. In particular, a natural choice is $\theta = \pi/2$, which gives a Dirac Hamiltonian in flat space of the form $H = -iv_F \hbar (\sigma_y \partial_x - \sigma_x \partial_y)$.

We now discuss a general argument which fixes the half integer offset of momentum quantization, and goes beyond the particular Dirac model chosen. Note, by time reversal invariance fixes this offset to be π or zero. In the latter case, a gapless one dimensional mode is present that is protected by time reversal symmetry. Now consider a slightly different geometry, an annular cylinder with radii R_1, R_2 . Take $R_2 \rightarrow \infty$ so we now have a hollow inner cylinder. If we now shrink the inner radius $R_1 \rightarrow 0$, one just obtains the bulk topological insulator. Hence, we must have that the modes on

the inner cylinder were gapped, which implies π phase shift. Note, although the cylinder is 'flat' in the sense it has vanishing Gaussian curvature, a nonzero spin connection leads to the Berry's phase of π . It is in this sense that we refer to this phase as being surface curvature induced - strictly it refers to a topological property of the surface (i.e. the possibility of looping around the cylinder while avoiding the inserted magnetic field).

2. *Model:* We use the Fu-Kane-Mele model of topological insulators on a diamond lattice Eq. 4 where the $\hat{\mathbf{d}}_{ik}^{1,2}$ are nearest neighbor unit vectors connecting a pair of second neighbor sites ik . We choose nearest neighbor hopping to be strong along direction (111) with strength $t_1 = 2t$ and the remaining three bonds to be of equal strength t . The spin orbit interaction is taken to be $\lambda_{SO} = 0.25t$. The 'cylinders' used for the computations are actually parallelepipeds, with the long axis z being along (110), and the cross section axes being along (011) and (101). Note, the single Dirac node at the surface of the long faces is located at $k_z = \pi$. This does not affect any of the results since this wavevector is along the propagation direction, and can be ignored. Note, symmetry of the diamond lattice relates the surface Dirac nodes along the two distinct surfaces, hence they are at the same energy. A more general situation is when there is no particular relation between the two - however, the topological properties should however remain unchanged, including the anomalous Aharonov-Bohm oscillations.

3. *Green's Function Calculation:* The matrix $\mathbf{G}_{1,N+1}^{(N+1)}(E)$, the Greens function between the first and last layers of a system with $N+1$ layers at energy E , where the matrix indices refer to sites in the layer. This can be efficiently calculated [13], assuming only nearest neighbor hopping between layers, denoted by the matrix \mathbf{t} and \mathbf{t}^\dagger . If the single layer Hamiltonian is \mathbf{H}_{N+1} , then the Greens function within this layer when attached to the remaining N layers is just:

$$\mathbf{G}_{N+1,N+1}^{(N+1)} = \left[(E + i\eta) - \mathbf{H}_{N+1} - \mathbf{t}^\dagger \mathbf{G}_{N,N}^{(N)} \mathbf{t} \right]^{-1} \quad (12)$$

$$\mathbf{G}_{1,N+1}^{(N+1)} = \mathbf{G}_{1,N}^{(N)} \mathbf{t} \mathbf{G}_{N+1,N+1}^{(N+1)} \quad (13)$$

where the energy label is suppressed. The last equation gives us the desired Greens function.

-
- [1] M. Z. Hasan and c. L. Kane, arXiv:1002.3895v1. X.-L. Qi and S.-C. Zhang, *Physics Today* 63, 33 (2010). J. E. Moore, *Nature* 464, 194 (2010).
- [2] C. L. Kane and E. J. Mele, *Phys. Rev. Lett.* 95, 226801 (2005).
- [3] R. A. Webb, S. Washburn, C. P. Umbach and R. B. Laibowitz, *Phys. Rev. Lett.* 54, 2696 (1985). V. Chandrasekhar, M. J. Rooks, S. Wind and D. E. Prober, *Phys. Rev. Lett.* 55, 1610 (1985).
- [4] A. D. Stone and Y. Imry, *Phys. Rev. Lett.* 56, 189 (1986).
- [5] B. L. Al'tshuler, A. G. Aronov and B. Z. Spivak, *Pis'ma Zh. Eksp. Teor. Fiz.* 33, 101 (1981) [*JETP Lett.* 33, 94 (1981)]. D. Yu. Sharvin and Yu. V. Sharvin, *Pis'ma Zh. Eksp. Teor. Fiz.* 34, 285 (1981) [*JETP Lett.* 34, 272 (1981)]. M. Gijs, C. van Haesendonck and Y. Bruynseraede, *Phys. Rev. Lett.* 52, 2069 (1984).
- [6] V. L. Nguyen, B. Z. Spivak and B. I. Shklovskii, *Pis'ma Zh. Eksp. Teor. Fiz.* 41, 35 (1985) [*JETP Lett.* 41, 42 (1985)]. Y. Avishai and R. Horowitz, *Phys. Rev. B* 35, 423426 (1987).
- [7] H. Peng, et al. *Nature Materials*, 9, 225-229 (2010)
- [8] Y. Zhang, Y. Ran, A. Vishwanath *Phys. Rev. B* 79, 245331 (2009).
- [9] See Supplementary Material.
- [10] D. H. Lee, *Phys. Rev. Lett.* 103, 196804 (2009).
- [11] Y. Ran, Y. Zhang and A. Vishwanath, *Nature Physics* 5, 298 (2009).
- [12] L. Fu, C.L. Kane and E. J. Mele, *Phys. Rev. Lett.* 98, 10680 (2007).
- [13] A. Croy, R. A. Roemer, M. Schreiber, in "Parallel Algorithms and Cluster Computing", (K. Hoffman, A. Meyer, eds.) Springer, Berlin, pp. 203-226 (2006) [cond-mat/0602300](#).
- [14] Y. Asada, K. Slevin and T. Ohtsuki, *Phys. Rev. B* 70, 035115 (2004)
- [15] K. Nomura, M. Koshino, S. Ryu, *Phys. Rev. Lett.* 99, 146806 (2007)
- [16] J. H. Bardarson, J. Tworzydło, P. W. Brouwer, C. W. J. Beenakker, *Phys. Rev. Lett.* 99, 106801 (2007).
- [17] T. Eguchi, P. Gilkey and A. Hansen, *Physics Reports* 66, 213 (1980).
- [18] J. Bardarson and J. Moore (to appear).